Astronomy & Astrophysics

Investigating the borderline between a young star cluster and a small stellar association: a test case with Bochum 1

E. Bica[1], C. Bonatto[1], and C. M. Dutra[2]

[1] Universidade Federal do Rio Grande do Sul, Departamento de Astronomia CP 15051, RS, Porto Alegre 91501-970, Brazil
e-mail: [charles;bica]@if.ufrgs.br
[2] Universidade Federal do Pampa – UNIPAMPA, Centro de Ciências da Saúde Rua Domingos de Almeida, 3525 Bairro São Miguel, Uruguaiana 97500-009, RS, Brazil
e-mail: cmdutra@gmail.com

ABSTRACT

Context. Usually, a loose stellar distribution can be classified as an OB stellar group, an association, or a young open cluster. We compare data with the typical OB association Vul OB1.
Aims. Here, we discuss the nature of Bochum 1, a typical example of an object affected by the above classification problem.
Methods. Field-decontaminated 2MASS photometry is used to analyse colour–magnitude diagrams (CMDs) and stellar radial density profiles (RDPs) of the structures present in the region of Bochum 1.
Results. The field-decontaminated CMD of Bochum 1 shows main sequence (MS) and pre-main sequence (PMS) stars. We report two new small angular-size, compact young clusters and one embedded cluster in the area of Bochum 1. Vul OB1 harbours the young open cluster NGC 6823 and the very compact embedded cluster Cr 404. The Vul OB1 association includes the H II region Sh2-86, and its stellar content is younger ($\approx$3 Myr) than that of Bochum 1 ($\approx$9 Myr), which shows no gas emission. Bochum 1 harbours one of the newly found compact clusters as its core. The RDP of Bochum 1 is irregular and cannot be fitted by a King-like profile, which suggests significant erosion or dispersion of stars from a primordial cluster. Similarly to Bochum 1, the decontaminated CMD of NGC 6823 presents conspicuous MS and PMS sequences. Taken separately, RDPs of MS and PMS stars follow a King-like profile. The core shows an excess density of MS stars that mimics the profile of a post-core collapse cluster. At such a young age, it can be explained by an excess of stars formed in the prominent core.
Conclusions. The present study suggests that Bochum 1 is a star cluster fossil remain that might be dynamically evolving into an OB association. Bochum 1 may be a missing link connecting early star cluster dissolution with the formation of low-mass OB associations.

Key words. open clusters and associations: general – Galaxy: structure

1. Introduction

Associations are loose stellar systems that may contain as many as 2600 stars, as in Cyg OB2 (Albacete Colombo et al. 2002; Knödlseder 2000). Although sharing a common origin and moving approximately in the same direction through the Galaxy, the member stars are gravitationally unbound. This definition encompasses a wide variety of objects, from the extended OB associations in spiral arms (Blaauw 1964) to the post-T Tauri associations in the Solar neighbourhood (e.g. Torres et al. 2000). OB associations can be observed over a wide range of distances from the Sun, from the relatively nearby ($\approx$140 pc) Scorpius-Centaurus Association (Maíz-Apellániz 2001) to the sparse and large ($\sim$400 pc) associations in the Large Magellanic Cloud and Andromeda (Efremov & Elmegreen 1998).

Most field stars appear to have been formed in stellar groups of different kinds, the OB associations in particular (Gomes et al. 1993; Massey et al. 1995). Rapid early gas removal is an efficient mechanism to drive cluster stars into the field and dissolve most of the very young star clusters on a time scale of 10–40 Myr, depending on cluster mass and star-formation efficiency (e.g. Goodwin & Bastian 2006). As a consequence of this, only about 5% (Lada & Lada 2003) of the embedded clusters are able to dynamically evolve into bound open clusters (OCs).

The above aspects raise the fundamental issue of the detection of dispersed cluster debris, and the distinction (if possible) between genuine small associations from dispersing debris. The present scenario, where early-cluster disruption is favoured, may provide clues to the dispersion of large star-forming complexes in the field, and remaining young OC families (Piskunov et al. 2006; de la Fuente Marcos & de la Fuente Marcos 2008).

Bochum 1 was defined by Moffat & Vogt (1975) as a group of 8 OB stars from the catalogue of Southern Luminous Stars (LS) by Stephenson & Sanduleak (1971). Moffat & Vogt (1975) carried out photoelectric observations with the ESO La Silla Bochum telescope, hence the object designation. They pointed out that the stars stand out from the background, and the colour–magnitude diagram (CMD) indicated a common reddening and distance. They derived $E(B-V) = 0.55 \pm 0.06$, $d_\odot = 4.06$ kpc and an O7 turn-off. Bochum 1 is located at $\ell = 193.43°$, $b = +3.40°$, and α(J2000) = $6^\mathrm{h}25^\mathrm{m}30^\mathrm{s}$ and δ(J2000) = $19°46'00''$.

Yadav & Sagar (2003) observed Bochum 1 with CCD photometry and referred to it as an OB association. They found that part of the bright stars in the area have a common proper motion, and a mass function that, within uncertainties, is comparable to that of Salpeter (1955). They derived $E(B-V) = 0.47 \pm 0.10$, $d_\odot = 2.8$ kpc, and an age of 10 Myr. Bochum 1 is included as a

star cluster in the WEBDA[1] database, which shows the values of Yadav & Sagar (2003).

Recently, Froebrich et al. (2007) presented a catalogue of star cluster candidates detected as stellar overdensities in the 2MASS[2] catalogue. FSR 911 was considered to be the same object as Bochum 1, but the positions are not coincident (Fig. 1).

In this context, the following interesting questions arise: is Bochum 1 a missing link between star clusters and stellar associations? Is it a dispersing fossil remain of a star cluster where scattered early-type stars and a remnant core are observed? Or is it a proto association that will eventually contain only scattered stars?

In a recent series of studies we coupled the classical CMD method with the analysis of the stellar radial density profile (RDP) to obtain intrinsic cluster astrophysical parameters and, in uncertain cases, to establish the nature of the objects (e.g. Bonatto & Bica 2008b; Bica et al. 2008; Bonatto & Bica 2007a; Bonatto & Bica 2007b; Bonatto et al. 2006b). Field decontamination was crucial in all these studies.

A previous discussion on the connection between massive young star clusters and a massive OB association was carried out by Knödlseder (2000) with Cyg OB2. In the present study we apply these methods to Bochum 1 and other low-mass stellar systems in the area. We also analyse NGC 6823 in Vul OB1, for comparison between young stellar systems.

This paper is structured as follows. In Sect. 2 we provide fundamental data on Bochum 1 and the other relevant stellar clusterings in its field, build the 2MASS CMDs and RDPs, and derive fundamental and structural parameters. In Sect. 3 we apply the above methods to the template young OC NGC 6823. In Sect. 4 we build mass functions and compute the stellar content. In Sect. 5 we discuss whether Bochum 1 is a genuine association or a dispersed young star cluster (or more than one). Concluding remarks are given in Sect. 6.

2. Stellar clusterings in the area of Bochum 1

Literature positions and the large angular dimensions of Bochum 1 and FSR 911 (Table 1) are shown schematically in Fig. 1. At first sight, the angular separation and dimensions suggest two large angular-size objects in the area. Inspection of wide-field XDSS[3] images of Bochum 1 and FSR 911 shows no evident stellar concentration such as an OC, nor gas emission.

However, when 2MASS (and XDSS) image close-ups were examined (Fig. 2), we found two very small compact clusters and an embedded cluster in the area (Table 1). They have not been reported in the literature. New Cluster 1 is located ≈1′ south of the nominal centre of FSR 911 (Table 1), while New Cluster 2 essentially coincides with the central position of Bochum 1 (Fig. 1). The embedded New Cluster 3 is located at the NE edge of the area (Fig. 1). The scattered OB stars that defined Bochum 1 (Moffat & Vogt 1975) are also shown in Fig. 1. Two of these stars are included in New Cluster 1, close to the west border of Bochum 1. Data for Bochum 1 OB members from Moffat & Vogt (1975) are given in Table 3, with equatorial coordinates
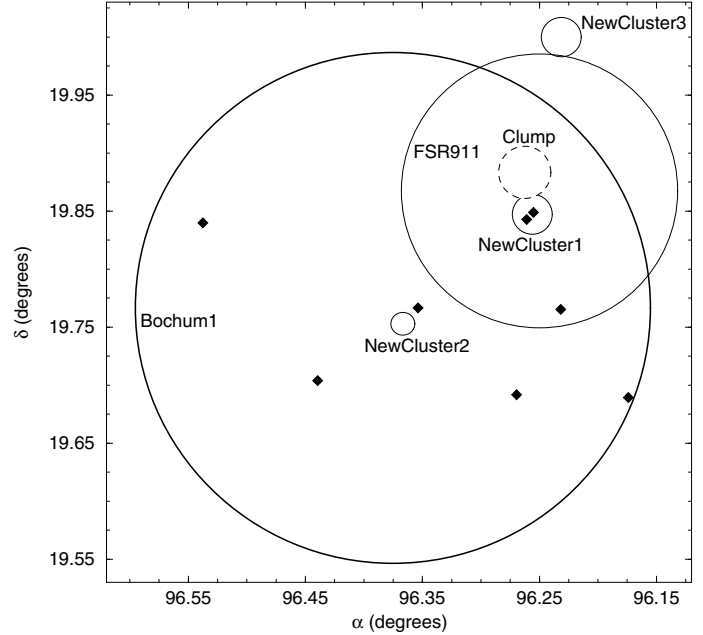

Fig. 1. Schematic view of a 30′ × 30′ field centred on Bochum 1. Objects in this field are centred on the coordinates given in Table 1, and are shown with the angular diameters given in Col. 5. The stars with spectral type determined by Moffat & Vogt (1975) are shown as diamonds.

and spectral types from SIMBAD[4]. LS46 and LS47 are members of New Cluster 1 (Fig. 1).

New Cluster 3 (Fig. 2) is looser and appears to be related to the IR source IRAS 06219+2258. New Cluster 1 is the richest one, while New Cluster 2 appears to be more populated than a multiplet of stars. Finally, Fig. 2 also shows a blowup of the possible core of the candidate cluster FSR 911. It shows New Cluster 1 to the south and a clump of faint stars to the north. The cell dimension for counting 2MASS stars in the FSR algorithm is 3.5′ × 3.5′ and the scan step is 20″ (Froebrich et al. 2007). Their derived core of FSR 911 must have included contributions of New Cluster 1 and the Clump (Fig. 1). A fundamental question is whether FSR 911, with its derived large tidal radius, actually exists as a cluster, an association or is just an artifact. Another important issue is to check hierarchically which small structure could be the core of a larger (Col. 9 of Table 1) one.

Molecular clouds, particularly giant ones, have multiple cores, some of them actively forming stars (e.g. Yonekura et al. 2005). The 3 small clusters in Table 1 might have been related to the cores of the early molecular cloud associated with Bochum 1.

2.1. CMD and structure of Bochum 1 and companions

Photometric properties were investigated by means of CMDs built with 2MASS data in the J, H and K_s bands. The extractions were performed with VizieR[5]. We follow the strategy described in Bonatto & Bica (2007b), and references therein, which is based on photometric extractions in wide circular fields for statistical representativity of cluster and field stars in terms of magnitude and colours. Only stars with errors in J, H and K_s smaller than 0.25 mag (a fraction of about 75%–85% of all stars – Bonatto & Bica 2007b) were considered.

---

[1] http://www.univie.ac.at/webda – Mermilliod & Paunzen (2003).
[2] The Two Micron All Sky Survey –
www.ipac.caltech.edu/2mass/releases/allsky/
[3] Extracted from the Canadian Astronomy Data Centre (CADC), at http://cadcwww.dao.nrc.ca/

[4] http://simbad.u-starsbg.fr/simbad/
[5] vizier.u-strasbg.fr/viz-bin/VizieR?-source=II/246

Table 1. General data on the star cluster/associations.

ℓ	b	$\alpha(2000)$	$\delta(2000)$	Diameter		R_{ext}	Designation	Comments
(°)	(°)	(hms)	(° ′ ″)	(′)	(pc)	(′)		
(1)	(2)	(3)	(4)	(5)	(6)	(7)	(8)	(9)
							The region of Bochum 1	
192.44	+3.41	6:25:30	+19:46:00	26.0^a	32^d	60	Bochum 1	
192.30	+3.36	6:25:00	+19:52:03	14.0^b	17^e	30	FSR 911	
192.64	+3.98	6:25:03	+19:53:00	2.5^c	3.1^e	30	Faint-star clump	Core of FSR 911?
192.31	+3.36	6:25:01	+19:50:55	1.0^c	1.3^d	30	New Cluster 1	Core of FSR 911? Includes LS46 and LS47
192.43	+3.40	6:25:28	+19:45:10	0.6^c	1.2^e		New Cluster 2	Core of Bochum 1? Includes LS51
192.17	+3.41	6:24:55	+19:59:59	1.0^c	1.3^d	30	New Cluster 3	Core of FSR 911? Includes IRAS 06219+2001
							The region of NGC 6823	
59.40	−0.14	19:43:09	+23:17:58	10.0	5.8^d	30	NGC 6823,Cr 405,OCl-124	
59.14	−0.11	19:42:28	+23:05:13	0.8	0.5^d	20	Cr 404,OCl-122	Embedded cluster, includes IRAS 19403+2258

Table Notes. Columns 1–4: central coordinates. Angular diameters (Col. 5) from: ^{a} the catalogue of Dias et al. (2002); ^{b} twice the tidal radius of Froebrich et al. (2007); ^{c} estimated in the present study from 2MASS K_s images. Absolute apparent diameters (Col. 6) computed with distances from the Sun from; ^{d} this work (Table 4); ^{e} assuming the same distance as that of Bochum 1. Column 7: 2MASS extraction radius.

We illustrate the procedure by means of the $J \times (J - H)$ and $J \times (J - K_s)$ CMDs of Bochum 1 (Fig. 3). When compared to the field stars (middle panels), the CMD extracted from the $R < 9'$ region of Bochum 1 (top) presents features that indicate a young age. However, it is evident that contamination by disk stars should be taken into account before conclusions on the intrinsic CMD morphology of Bochum 1 are made.

2.2. Field-star decontamination

Although difficult, field-star decontamination is important to characterise and derive parameters of star clusters. Several different approaches have been used for this, among them those of Mercer et al. (2005) and Carraro et al. (2006). The first is based on spatial variations of the star-count density, but does not take into account colour and magnitude properties. In the latter, stars of a CMD extracted from an assumed cluster region are subtracted according to colour and magnitude similarity with the stars of an equal-area comparison field CMD.

In the present case, we apply the statistical algorithm described in Bonatto & Bica (2007b) to quantify the field-star contamination in the CMDs. The algorithm makes use of both approaches above, in the sense that relative star-count density together with colour/magnitude similarity between cluster and comparison field are taken into account simultaneously. It measures the relative number densities of probable field and cluster stars in cubic CMD cells whose axes correspond to the J magnitude and the $(J - H)$ and $(J - K_s)$ colours. These are the 2MASS colours that provide the maximum variance among CMD sequences for OCs of different ages (e.g. Bonatto et al. 2004). The algorithm: (i) divides the full range of magnitude and colours covered by the CMD into a 3D grid, (ii) calculates the expected number density of field stars in each cell based on the number of comparison field stars with similar magnitude and colours as those in the cell; and (iii) subtracts the expected number of field stars from each cell. The algorithm is responsive to local variations of field-star contamination (Bonatto & Bica 2007b). Cell dimensions used here are $\Delta J = 1.0$, and $\Delta(J - H) = \Delta(J - K_s) = 0.25$, which are large enough to allow sufficient star-count statistics in individual cells and small enough to preserve the morphology of the CMD evolutionary

sequences. For representative background star-count statistics we use the ring located within $R_{inf} \leq R \leq R_{ext}$ around the cluster centre as the comparison field, where R_{inf} usually represents twice the RDP radius (Sect. 2.4). We emphasise that the equal-area field extractions shown in the middle panels of Figs. 3 to 5 and 9 serve only for comparisons among the panels. Actually, the decontamination process is carried out with the large surrounding area as described above.

As extensively discussed in Bonatto & Bica (2007b), differential reddening between cluster and field stars is critical for the decontamination algorithm. Large gradients would require large cell sizes or, in extreme cases, preclude application of the algorithm altogether. A $|\Delta(J - H)| \gtrsim$ cell size (0.25, in the present work) would be required between cluster and comparison field for the differential reddening to affect the subtraction in a given cell. However, in the present cases the CMDs extracted from the cluster region and comparison field (Figs. 3 to 5 and 9) indicate that the differential reddening is not important.

The decontaminated CMDs are shown in the bottom panels of Figs. 3 to 5 and 9. As expected, most of the contamination is removed, leaving stellar sequences typical of young OCs, with a nearly vertical main sequence (MS), and evidence of a large fraction of pre-MS stars, especially in Bochum 1 (Fig. 3) and NGC 6823 (Fig. 9). For illustrative purposes, we provide in Table 2 the full statistics of the decontamination process applied to the region $R < 9'$ of Bochum 1, by magnitude bins. Statistically relevant parameters to characterise the nature of a star cluster are: (i) $N_{1\sigma}$ which, for a given magnitude bin, corresponds to the ratio of the decontaminated number of stars to the 1σ Poisson fluctuation of the number of observed stars; (ii) σ_{FS}, which is related to the probability that the decontaminated stars result from the normal star count fluctuation in the comparison field and; (iii) FS_{unif}, which measures the star-count uniformity of the comparison field. Properties of $N_{1\sigma}$, σ_{FS}, and FS_{unif}, measured in OCs and field fluctuations, are discussed in Bica et al. (2008). Table 2 also provides integrated values of the above parameters, which correspond to the full magnitude range spanned by the CMD. The spatial region considered here is that sampled by the CMDs shown in the top panels of Fig. 3.

Star cluster CMDs should have integrated $N_{1\sigma}$ values significantly larger than 1 (Bica et al. 2008), a condition that is fully
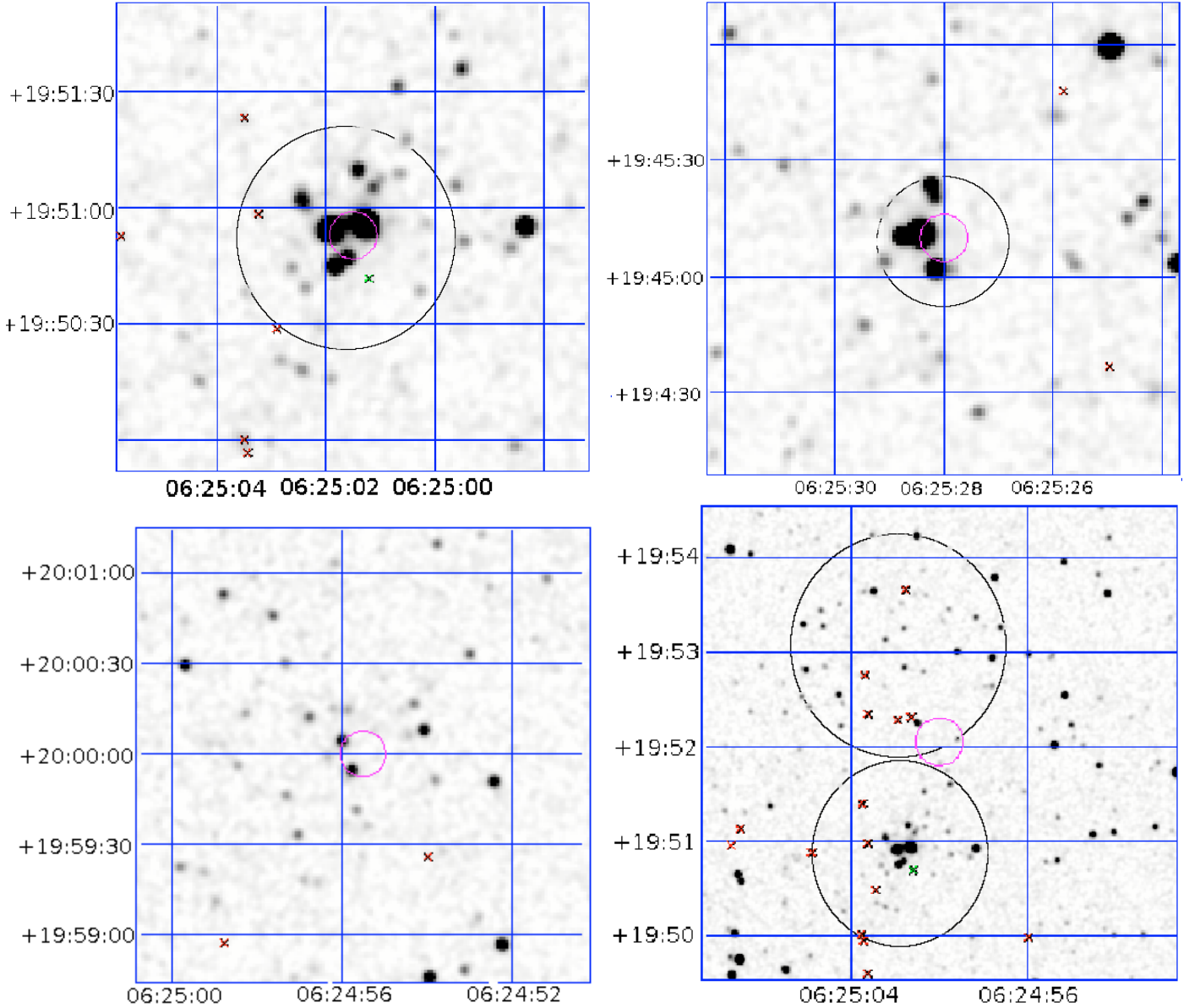
Fig. 2. *Top left*: 2′ × 2′ 2MASS K_s image of New Cluster 1; the large circle corresponds to the RDP radius (Table 5). *Top right*: 2′ × 2′ 2MASS K_s image of New Cluster 2; the apparent diameter (Table 1) is shown by the large circle. *Bottom left*: 2′ × 2′ 2MASS K_s image of New Cluster 3. The RDP radius encompasses the image (Table 5). *Bottom right*: 3′ × 3′ 2MASS K_s image of the central region of FSR 911; the large circle to the North corresponds to the apparent diameter of the faint clump (Table 1), and the south one to the RDP radius (Table 5). Images provided by the 2MASS Image Service. The small circles indicate the central coordinates (Cols. 3 and 4 of Table 1). Figure orientation: *North to the top and East to the left.*

met by Bochum 1, with $N_{1\sigma} = 9.4$. As a further test of the statistical significance of the above results we investigate star count properties of the field stars. First, the comparison field is divided into 8 sectors around the cluster centre. Next, we compute the parameter σ_{FS}, which is the 1σ Poisson fluctuation around the mean of the star counts measured in the 8 sectors of the comparison field (corrected for the different areas of the sectors and cluster extraction). In a spatially uniform comparison field, σ_{FS} is expected to be small. In this context, star clusters should have a probable number of member stars (N_{cl}) higher than $\sim\sigma_{FS}$, to minimise the probability that N_{cl} arises from fluctuations of a non-uniform comparison field. This condition is fully satisfied, in some cases reaching the level $N_{cl} \sim 4\,\sigma_{FS}$. Finally, we also provide in Table 2 the parameter FS_{unif}. For a given magnitude

bin we first compute the average number of stars over all sectors $\langle N \rangle$ and the corresponding 1σ fluctuation $\sigma_{\langle N \rangle}$; thus, FS_{unif} is defined as $FS_{unif} = \sigma_{\langle N \rangle}/\langle N \rangle$. Non uniformities such as heavy differential reddening should result in high values of FS_{unif}.

Since we usually work with comparison fields larger than the possible-cluster extractions, the correction for the different spatial areas between field and cluster is expected to produce a fractional number of probable field stars (n_{fs}^{cell}) in some cells. Before the cell-by-cell subtraction, the fractional numbers are rounded off to the nearest integer, but limited to the number of observed stars in each cell, $n_{sub}^{cell} = NI(n_{fs}^{cell}) \leq n_{obs}^{cell}$, where NI represents rounding off to the nearest integer. The global effect is quantified by means of the difference between the expected number of field stars in each cell (n_{fs}^{cell}) and the actual number of subtracted

Table 2. Field-star decontamination statistics.

ΔJ	Bochum 1 ($R < 9'$)				
	N_{obs}	N_{cl}	$N_{1\sigma}$	σ_{FS}	FS_{unif}
(mag)	(stars)	(stars)		(stars)	
8–9	4 ± 2.0	3	1.5	1.34	0.91
9–10	10 ± 3.2	4	1.3	2.00	0.49
10–11	11 ± 3.3	3	0.9	2.23	0.22
11–12	31 ± 5.6	9	1.6	4.38	0.21
12–13	52 ± 7.2	10	1.4	3.61	0.07
13–14	100 ± 10.0	4	0.4	8.94	0.09
14–15	212 ± 14.6	30	2.1	19.385	0.10
15–16	499 ± 22.3	144	6.4	38.50	0.10
16–17	450 ± 21.2	139	6.6	94.11	0.33
8–17	1369 ± 37.0	346	9.4	137.3	0.13

Table notes. The upper lines give the statistics in each magnitude bin, while the integrated values are in the bottom line. See text for details on parameters.

Table 3. Bochum 1 members according to Moffat & Vogt (1975).

Star	$\alpha(2000)$	$\delta(2000)$	Spectral type
	(hms)	(° ′ ″)	
(1)	(2)	(3)	(4)
LS 44	06:24:38.4	+19:42:16	O7.5V
LS 45	06:24:55.6	+19:45:55	B1.5V
LS 46	06:25:01.2	+19:50:56	B
LS 47	06:25:01.8	+19:50:54	B0
LS 48	06:25:04.7	+19:41:30	G5
LS 51	06:25:24.9	+19:46:00	B
LS 53	06:25:45.5	+19:42:14	F5
LS 54	06:26:09.0	+19:50:24	–

Table notes. Coordinates and spectral types from SIMBAD.

stars (n_{sub}^{cell}). Summed over all cells, this quantity provides an estimate of the total subtraction efficiency of the process,

$$f_{sub}(\%) = 100 \times \sum_{cell} n_{sub}^{cell} \Big/ \sum_{cell} n_{fs}^{cell}.$$

Ideally, the best results would be obtained for an efficiency $f_{sub} \approx 100\%$. With the assumed grid settings, the decontamination efficiency turned out to be higher than 96% in all cases dealt with in this paper.

2.3. Fundamental parameters

The young-age features of Bochum 1 are enhanced in the decontaminated CMDs (bottom panels of Fig. 3), especially a poorly-populated main sequence (MS) and a significant number of pre-main sequence (PMS) stars. Solar-metallicity isochrones from the Padova group (Girardi et al. 2002) computed with the 2MASS filters, and the PMS tracks of Siess et al. (2000) are used to characterise the age and compute fundamental parameters. Reddening transformations are $A_J/A_V = 0.276$, $A_H/A_V = 0.176$, $A_{K_S}/A_V = 0.118$, and $A_J = 2.76 \times E(J - H)$ (Dutra et al. 2002), for a constant $R_V = 3.1$, which are based on the extinction curve of Cardelli et al. (1989).
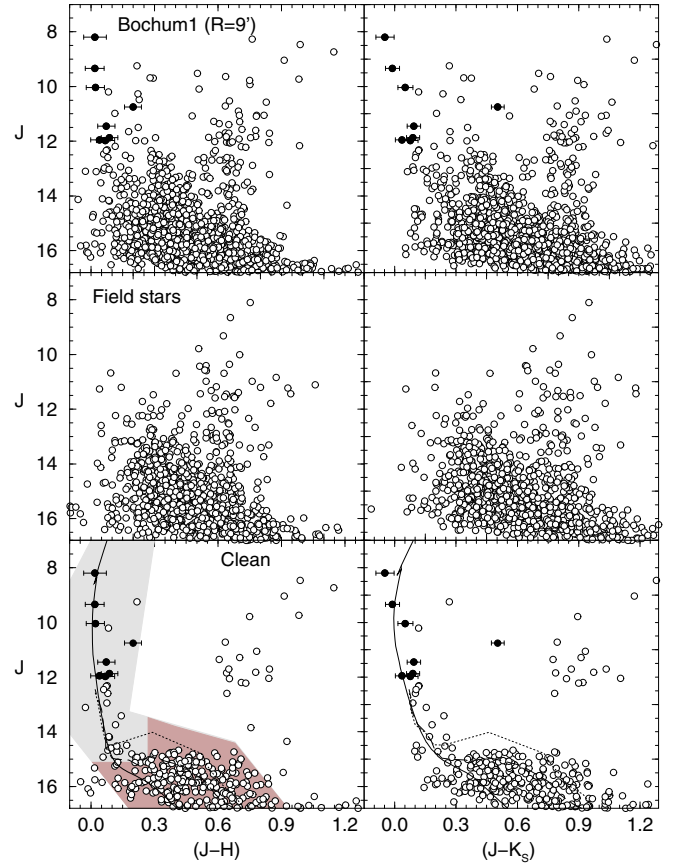

Fig. 3. 2MASS CMDs extracted from the $R < 9'$ region of Bochum 1. *Top panels*: observed photometry with the $J \times (J - H)$ (*left*) and $J \times (J - K_s)$ colours (*right*). *Middle*: equal-area comparison field extracted from the region 49′.18–50′. *Bottom panels*: decontaminated CMDs showing a poorly-populated MS and a significant number of PMS stars. Also shown are the 9 Myr Padova isochrone (solid line) together with the 5 Myr (dashed) and 10 Myr (dotted) PMS tracks (Siess et al. 2000). Light-shaded polygon: colour–magnitude filter to isolate the MS stars. Heavy-shaded polygon: colour–magnitude filter for the PMS stars. Stars with spectral type determined by Moffat & Vogt (1975) are shown as filled circles. Error bars are not shown to avoid cluttering.

The best-fit was obtained with the 9 Myr isochrone, apparent distance modulus $(m - M)_J = 13.4 \pm 0.1$, and $E(J - H) = 0.11 \pm 0.02$, which converts to $E(B - V) = 0.35 \pm 0.06$ and $A_V = 1.1 \pm 0.2$. Considering fit uncertainties, the age of Bochum 1 can be set at 9 ± 3 Myr, consistent with the values of Moffat & Vogt (1975) and Yadav & Sagar (2003). The absolute modulus is $(m - M)_O = 13.1 \pm 0.1$, and the distance from the Sun $d_\odot = 4.2 \pm 0.1$ kpc. Within uncertainties, this value of $d_\odot$ agrees with that of Moffat & Vogt (1975), but it is ≈50% larger than the value of Yadav & Sagar (2003). The 5 Myr and 10 Myr PMS tracks set with the above reddening and distance modulus overlap most of the faint ($J \gtrsim 15$) and red (($J - H) \gtrsim 0.3$) stars, which results in an age of ≈9 Myr for Bochum 1. This isochrone solution is shown in the bottom panels of Fig. 3. CMDs in both colours present comparable results.

The presently derived fundamental parameters are given in Table 4, where we also provide the Galactocentric distance (R_{GC}), which is based on the recently derived value of the Sun's distance to the Galactic centre $R_\odot = 7.2$ kpc, computed by means of Globular clusters (Bica et al. 2006).
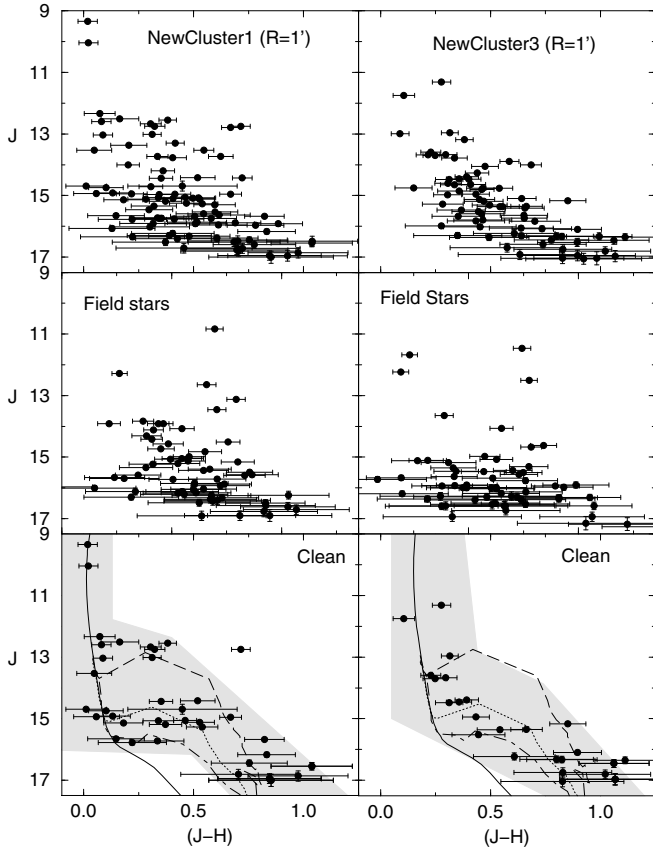
Fig. 4. Same as Fig. 3 for the $J \times (J - H)$ CMDs of the $R < 1'$ regions of New Cluster 1 (*left panels*) and New Cluster 3 (*right*). Isochrones used for New Cluster 1 are the Padova 7 Myr (solid line), and the 1 Myr (dashed), 5 Myr (dotted) and 10 Myr (long-dashed) PMS tracks (Siess et al. 2000). The same isochrone setting was used to characterise the age of New Cluster 3.

Fig. 5. Same as Fig. 3 for the $J \times (J - H)$ CMDs of the $R < 1'$ region of New Cluster 2 (*left panels*) and the $R < 1\overset{'}{.}25$ region of the stellar clump in the region of FSR 911 (*right*).

The remaining objects in the field of Bochum 1 (Fig. 1) were analysed in the same way. Their fundamental parameters are given in Table 4.

Similarly to Bochum 1, the CMD of New Cluster 1 shows features of a young age (Fig. 4). Because of the presence of brighter MS and PMS stars, it appears to be slightly younger than Bochum 1. PMS tracks with ages 1 Myr, 5 Myr, and 10 Myr provide a reasonable description of the red and faint stellar distribution (bottom-left panel of Fig. 4). We estimate an age of 7 ± 3 Myr, $(m - M)_J = 13.7 \pm 0.1$, $E(J - H) = 0.15 \pm 0.01$, $(m - M)_O = 13.3 \pm 0.1$ and $d_\odot = 4.5 \pm 0.2$ kpc, which agrees with the distance from the Sun of Bochum 1 (Table 4).

The poorly-populated decontaminated CMD of New Cluster 3 (bottom-right panel of Fig. 4) does not provide enough constraints for an independent isochrone fit. In this case we simply use the isochrone solution of New Cluster 1 to test whether it is acceptable. Parameters derived in this way are $(m - M)_J = 13.9 \pm 0.2$, $E(J - H) = 0.26 \pm 0.02$, $(m - M)_O = 13.2 \pm 0.2$ and $d_\odot = 4.3 \pm 0.4$ kpc, similar to that of Bochum 1 (Table 4).

Finally, in Fig. 6 we examine how the isochrone fit uncertainties affect the quality of the adopted solution. It shows, for the 4 cases with fundamental parameters and errors derived in the present work (Table 4), the adopted Padova isochrone solution to the MS together with the solutions produced by the 1σ-variations applied to the adopted age, reddening and distance modulus. With 3 independent parameters and 3 different values
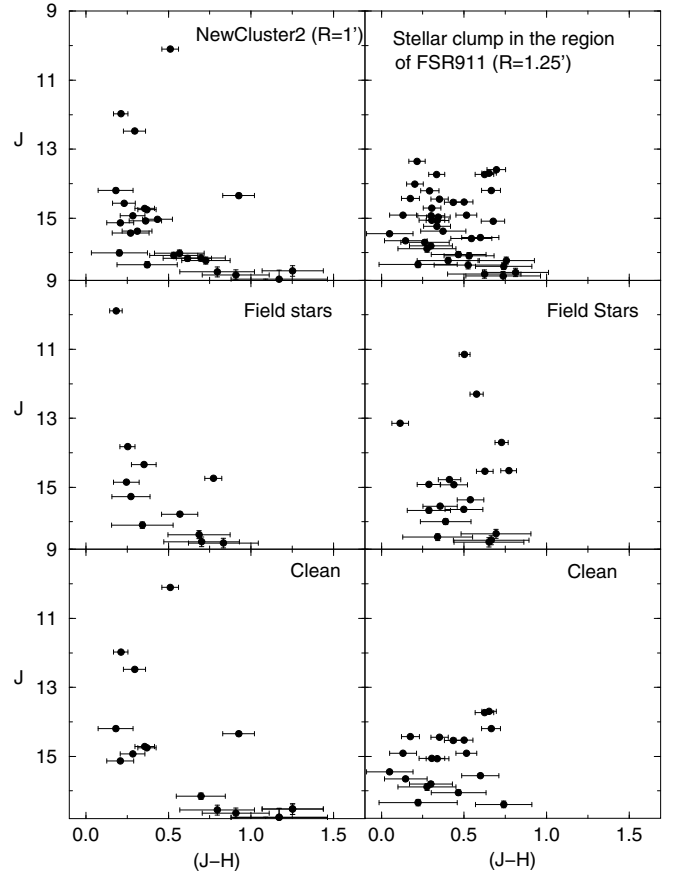
each, a total of 27 solutions were taken into account. Thus, for clarity we show in Fig. 6 the *best-fit* together with the envelope of solutions. Note that NGC 6823 is analysed in Sect. 3.1. Since the objects shown in Fig. 6 are very young, most of their stellar content, especially the red ones, should correspond to the PMS phase. Indeed, Fig. 6 also shows that the colour range spanned by these red stars cannot be accounted for by uncertainties associated with the MS isochrone fit.

2.4. Cluster structure

We examine the structure of the above objects by means of the projected radial distribution of the number density of stars around the centre. We work with RDPs built with colour-magnitude filtered (bottom panels of Figs. 3, 4, and 9) photometry, which minimises contamination of non-cluster stars and produces more intrinsic profiles (e.g. Bonatto & Bica 2007b, and references therein). To describe the RDPs we use the analytical profile $\sigma(R) = \sigma_{bg} + \sigma_0/(1 + (R/R_C)^2)$, where σ_{bg} is the residual background density, σ_0 is the central density of stars, and R_C is the core radius. This function is similar to the King (1962) profile usually applied to the central parts of globular clusters.

The RDPs of Bochum 1, New Cluster 1, and New Cluster 3 are shown in Fig. 7 (left panels). Bochum 1, in particular, has a low-contrast profile disturbed by the presence of New Cluster 1 and the possible presence of FSR 911. As a result, this irregular RDP cannot be fitted with the adopted King-like profile. New Cluster 2 fits right into the central bin of the RDP of

Table 4. Fundamental parameters derived in this work.

Object	Age (Myr)	A_V (mag)	$d_\odot$ (kpc)	R_{GC} (kpc)	x_{GC} (kpc)	y_{GC} (kpc)	z_{GC} (kpc)
(1)	(2)	(3)	(4)	(5)	(6)	(7)	(8)
Bochum 1	9 ± 3	1.1 ± 0.2	4.2 ± 0.2	11.3 ± 0.2	-11.3 ± 0.2	-0.88 ± 0.02	$+0.25 \pm 0.02$
New Cluster 1	7 ± 3	1.5 ± 0.1	4.5 ± 0.2	11.7 ± 0.2	-11.6 ± 0.2	-0.97 ± 0.05	$+0.27 \pm 0.02$
New Cluster 3[†]	7 ± 3	2.6 ± 0.2	4.3 ± 0.4	11.5 ± 0.4	-11.5 ± 0.4	-0.91 ± 0.09	$+0.26 \pm 0.02$
NGC 6823	4 ± 2	2.7 ± 0.1	2.0 ± 0.1	6.4 ± 0.1	-6.2 ± 0.2	$+1.76 \pm 0.04$	0.00 ± 0.01

Table notes. Column 2: age derived in this paper with 2MASS data. Column 3: $A_V = 3.1 \, E(B-V)$. Column 4: distance from the Sun. Column 5: galactocentric distance calculated with $R_\odot = 7.2$ kpc (Bica et al. 2006) as the distance of the Sun to the Galactic centre. Columns 6–8: positional components with respect to the Galactic plane. (†): parameters computed for the same isochrone solution as New Cluster 1.
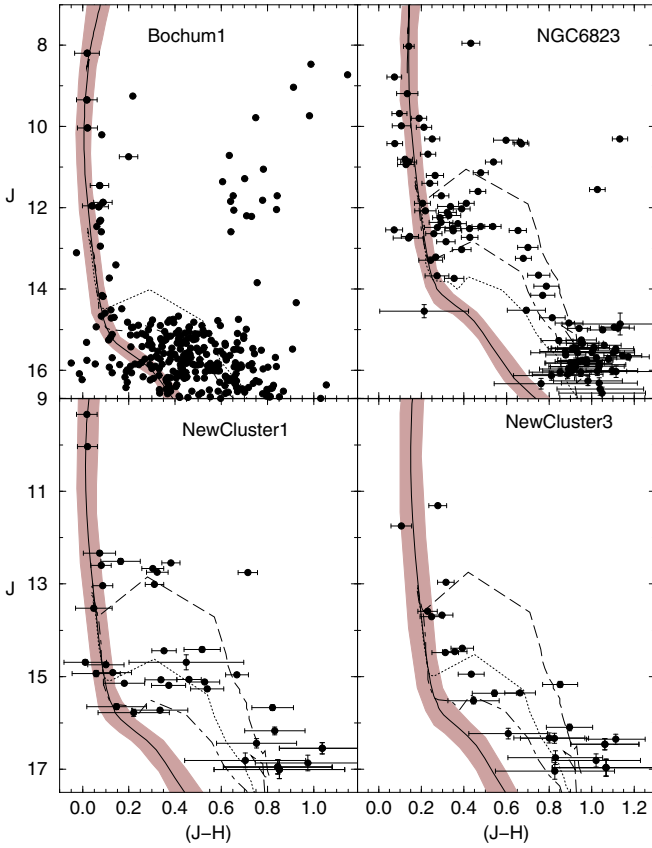

Fig. 6. Effects of propagating the 1σ-uncertainties in age, reddening, and distance modulus (Table 4), into the adopted Padova isochrone solution to the MS of Bochum 1, NGC 6823, New Cluster 1 and 3. Field-decontaminated CMDs are used in all cases. Parameter variations are enveloped by the shaded polygons.

Fig. 7. Stellar RDPs (filled circles) built with colour–magnitude photometry. The best-fit King-like profile is shown as a solid line in panels **b)**, **d)**–**g)**, where the background level (horizontal shaded polygon) and the 1σ King fit uncertainty (gray region) are also shown. The RDPs of Bochum 1 **a)** and the stellar clump in the region of FSR 911 **c)** cannot be fitted. RDPs built with the MS **f)** and PMS **g)** stars of NGC 6823 are shown separately. Angular scale is used.

Bochum 1 (Fig. 7, panel a). Despite the irregularities, this RDP still presents a density gradient decreasing for larger radii.

New Cluster 1 and New Cluster 3, on the other hand, have profiles that, despite bumps due to neighbouring objects, follow the King-like function, especially the former. To arrive at the fits shown in Fig. 7, the RDP points that correspond to other objects were excluded. We also estimate the cluster RDP radius R_{RDP}, which corresponds to the distance from the cluster centre where RDP and background become statistically indistinguishable (e.g. Bonatto & Bica 2005). For the purposes of the present work, we adopt R_{RDP} as the cluster size.

The structural parameters derived as described above are given in Table 5, where we also include the density contrast
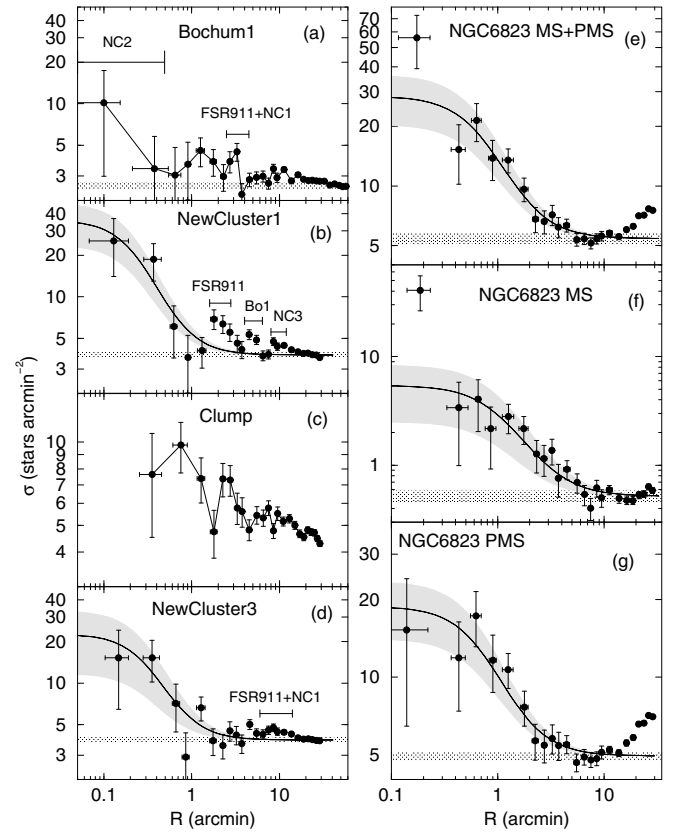
parameter $\delta_c = 1 + \sigma_0/\sigma_{bg}$. As expected from the RDPs in Fig. 7, Bochum 1 presents the lowest contrast profile among the objects in that region.

3. NGC 6823: a nearby template of a young open cluster

NGC 6823 has been studied by Barkhatova (1957) and more recently by Kharchenko et al. (2005). The latter authors derive the age of 10 Myr, $E(B-V) = 0.84$, $d_\odot = 1.9$ kpc, $R_C = 4'.2$, and a cluster radius $R_{clus} = 16'.2$. WEBDA provides $E(B-V) = 0.85$,

Table 5. Structural parameters measured in the RDPs built with colour–magnitude filtered photometry.

Cluster	1′	σ_{bg}	RDP						
	(pc)	(stars arcmin^{-2})	σ_0 (stars arcmin^{-2})	δ_c	R_C (′)	R_{RDP} (′)	R_C (pc)	R_{RDP} (pc)
(1)	(2)	(3)	(4)	(5)	(6)	(7)	(8)	(9)
Bochum 1	1.309	2.6 ± 0.1	–	–	–	18 ± 2	–	23 ± 3
New Cluster 1	1.317	3.8 ± 0.1	32 ± 12	9.4 ± 3.1	0.23 ± 0.08	1.0 ± 0.1	0.30 ± 0.10	1.3 ± 0.1
New Cluster 3[†]	1.256	3.9 ± 0.1	18.7 ± 10.8	5.8 ± 2.8	0.31 ± 0.15	2.0 ± 0.2	0.39 ± 0.19	2.5 ± 0.3
NGC 6823[a]	0.593	5.4 ± 0.1	23.0 ± 7.9	4.2 ± 0.3	0.74 ± 0.19	5.0 ± 0.5	0.43 ± 0.11	3.0 ± 0.3
NGC 6823[b]	0.593	0.5 ± 0.1	4.9 ± 2.9	10.4 ± 3.2	0.97 ± 0.43	7.0 ± 1.0	0.57 ± 0.25	4.1 ± 0.6
NGC 6823[c]	0.593	4.9 ± 0.1	13.9 ± 4.7	3.8 ± 0.9	0.77 ± 0.21	5.0 ± 1.0	0.46 ± 0.12	3.0 ± 0.6

Table notes. Column 2: arcmin to parsec scale. To minimise degrees of freedom in RDP fits with the King-like profile (see text), σ_{bg} was kept fixed (measured in the respective comparison fields) while σ_0 and R_C were allowed to vary. Column 5: cluster/background density contrast ($\delta_c = 1 + \sigma_0/\sigma_{bg}$), measured in colour–magnitude filtered RDPs. (†): absolute values computed for the same isochrone solution of New Cluster 1. [a] measured in the RDP that includes MS and PMS stars. [b] MS stars only. [c] PMS stars only.

$d_\odot$ = 1.9 kpc and an age of 6 Myr. We use NGC 6823 as a relatively nearby template OC. It has a prominent core (Pigulski et al. 2000), and the small embedded cluster Cr 404 is projected not far from NGC 6823. NGC 6823 and Cr 404 are part of the association Vul OB1 with a diameter of 170′ × 130′. Massey et al. (1995) studied NGC 6823/Vul OB1 deriving an average reddening $E(B - V)$ = 0.89, a distance $d_\odot$ = 2.3 kpc and ages in the range 2–7 Myr. The H II region Sh2-86 (Sharpless 1959) with an angular diameter of 40′ is included in Vul OB1. The kinematic distance of Sh2-86 is 1.9 kpc (Brand & Blitz 1993).

Cr 404 was first recognised as a star cluster by Collinder (1931). It is embedded in the small angular size nebula NGC 6820. In modern classifications it is a typical embedded cluster (Hodapp 1994). It is projected just outside NGC 6823. A 2MASS K_s image of the embedded cluster Cr 404 in the nebula NGC 6820 is shown in Fig. 8. We conclude that the Vul OB1 complex shows an OC with a prominent core and an embedded cluster with hardly any trace of a halo. It is extremely compact and unresolved by 2MASS photometry. Cr 404 requires a large telescope for a deeper analysis.

3.1. CMD and structure of NGC 6823

We apply to NGC 6823 the same analysis as for Bochum 1 (Sect. 2.1). The $J \times (J - H)$ CMD extracted from the $R < 3'$ of NGC 6823 is shown in Fig. 9. A conspicuous, nearly-vertical MS can be seen in the decontaminated CMD (bottom-left panel), together with a group of faint and red PMS stars. Such CMD morphology can be well described with a 4 Myr Padova isochrone and the 1 Myr, 5 Myr, and 10 Myr PMS tracks. Acceptable fits are obtained with ages in the range 2–7 Myr. The fit in Fig. 9 was obtained for $(m - M)_J$ = 12.3 ± 0.1, $E(J - H)$ = 0.27 ± 0.01, which converts to $E(B - V)$ = 0.86 ± 0.06 and A_V = 2.7 ± 0.2. The absolute modulus is $(m - M)_O$ = 11.5 ± 0.1, and the distance from the Sun is $d_\odot$ = 2.0 ± 0.1 kpc (Table 4). These values agree with those in Kharchenko et al. (2005) and WEBDA.

The RDPs of NGC 6823 are shown in Fig. 7. Besides the RDP that includes MS and PMS stars, we also consider both stellar distributions separately. The King-like function describes well most of the profiles, except for the innermost radial bin in the MS and MS+PMS RDPs, which indicates an excess of MS stars near the cluster centre ($R \lesssim 0.2' \approx 0.1$ pc). This feature
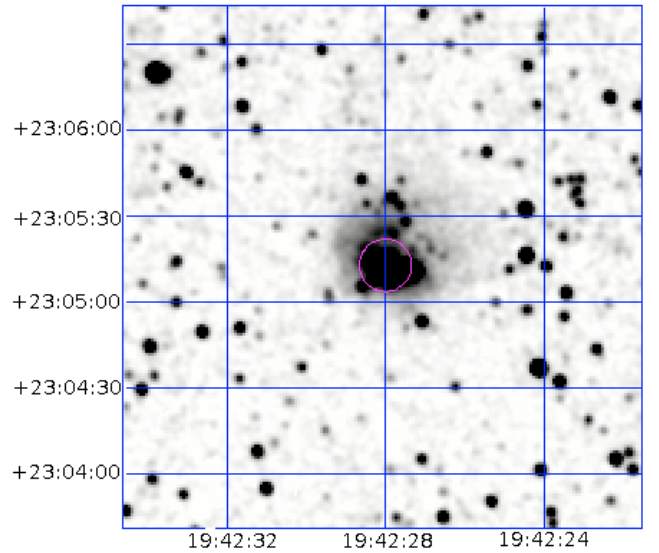

Fig. 8. 3′ × 3′ 2MASS K_s image of the embedded cluster Cr 404 in the nebula NGC 6820. Figure orientation: *North to the top and East to the left*.

is characteristic of post-core collapse globular clusters (Trager et al. 1995). We note that a post-core collapse feature in the RDP of OCs has been previously detected, for instance, in the ~1 Gyr old cluster NGC 3960 (Bonatto & Bica 2006). However, at the young age of NGC 6823, a possible explanation for the central stellar density is an enhanced fragmentation in the central parts of the parent molecular cloud, and/or primordial dynamical evolution. Another conspicuous feature is the excess of PMS stars for $R \gtrsim 10'$.

4. Mass functions and stellar content

For a deeper analysis of the stellar distribution we build mass functions (MFs) for the MS stars with the J, H, and K_s bands independently (see, e.g. Bonatto & Bica 2005). The MFs of Bochum 1, New Cluster 1, and NGC 6823 are built with the stars isolated with the respective colour–magnitude filters (Figs. 3, 4, and 9), which minimise contamination by field stars (e.g. Bonatto & Bica 2007b). In all cases we consider the full radial
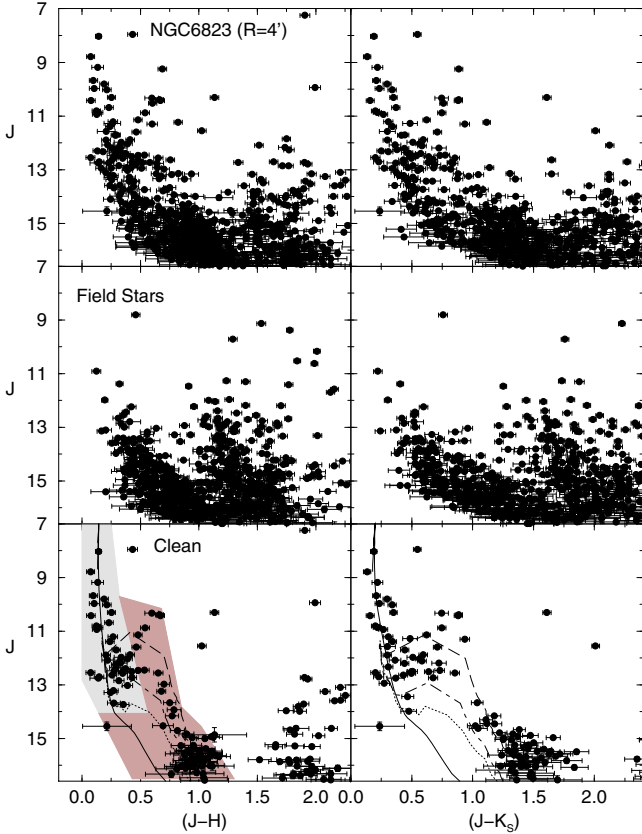
Fig. 9. Same as Fig. 3 for the $R < 4'$ region of NGC 6823. The isochrones (*bottom-left*) used are the 4 Myr (Padova) and the PMS tracks of 1 Myr (dashed line), 5 Myr (dot-dashed), and 10 Myr (dotted). Light-shaded polygon: colour–magnitude filter to isolate the MS stars. Heavy-shaded polygon: colour–magnitude filter for the PMS stars.
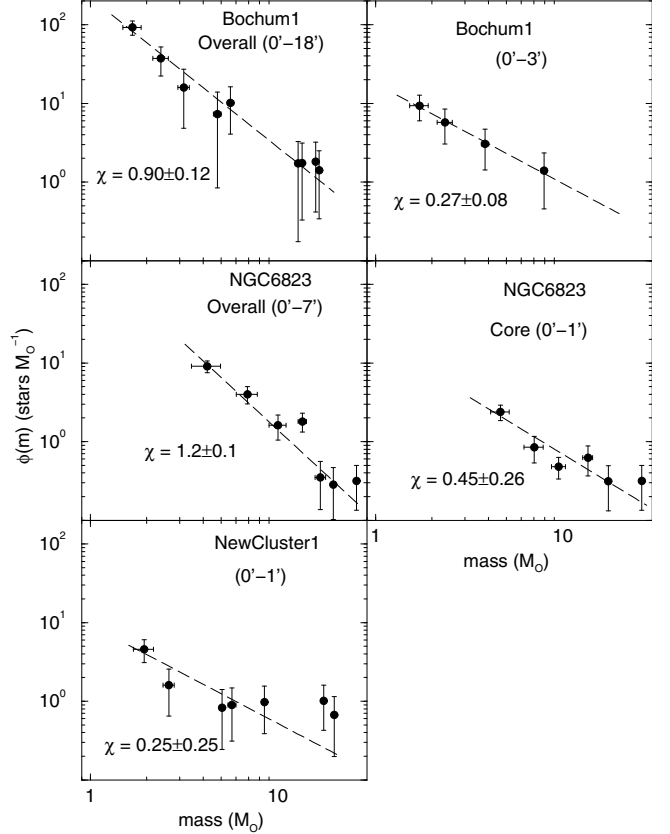

Fig. 10. Mass functions of Bochum 1 (*top panels*), NGC 6823 (*middle*), and New Cluster 1 (*bottom*). The *left panels* show the MF derived for the whole cluster region, while the *right ones* contain the MF for the inner region, the core in the case of NGC 6823. The dashed line shows the mass function fit.

extent of the objects and inner regions, the core in the case of NGC 6823. The MFs are shown in Fig. 10. The MS mass ranges are 1.5–17 $M_\odot$ for Bochum 1, 3.5–27 $M_\odot$ for NGC 6823, and 1.3–21 $M_\odot$ for New Cluster 1.

The MFs are well described by the function $\phi(m) = \phi_0\, m^{-(1+\chi)}$. With $\chi \approx 0.9$, the overall MF of Bochum 1 (top panels) is somewhat flatter than the slope $\chi = 1.35$ of the Salpeter (1955) initial mass function (IMF). However, the MF extracted for an inner region ($R < 3'$) shows an even flatter slope, $\chi \approx 0.3$. Such flat values, especially the inner one, reflect large-scale mass segregation in this young object, which suggests primordial dynamical evolution and/or star-forming effects (e.g. Bonatto & Bica 2005).

A similar picture applies to NGC 6823 (middle panels), although in this case the overall MF slope approaches the Salpeter one. We note that the present overall slope is steeper than that derived by Massey et al. (1995), $\chi = 0.3$. New Cluster 1 also presents a flat MF slope, $\chi \approx 0.25$ (bottom).

In Table 6 we quantify the stellar content for Bochum 1, NGC 6823, and New Cluster 1. We consider MS and PMS stars separately (for simplicity we assume a canonical mass of 1 $M_\odot$ for the PMS stars). We estimate that only $\approx$23% of the stars in Bochum 1 have already reached the MS. MS and PMS stars taken together, the mass of Bochum 1 is $\approx$720 $M_\odot$. In NGC 6823 the fractions of MS and PMS stars are more evenly distributed. It is more massive than Bochum 1, with a mass of about 1150 $M_\odot$. New Cluster 1 has a small number of MS and PMS stars ($\approx$20), which results in a very low mass of $\approx$74 $M_\odot$.

Crowding and completeness should not be important for the above arguments, because these objects are mostly poorly-populated and sparse, and besides, faint MS stars are not included in the colour–magnitude filters (Figs. 3, 4, and 9).

Finally, in Fig. 11 we compare the presently measured age and mass values for Bochum 1, New Cluster 1, and NGC 6823 with those derived by Piskunov et al. (2008)[6] for a relatively large sample of nearby OCs. Our mass value for NGC 6823 (Table 6) is about half that estimated by Piskunov et al. (2008) which, considering the different methods, can be taken as a reasonable agreement. Based on the mass distribution of the clusters with any age (panel b), the genuine young OC NGC 6823 is more massive than the average cluster mass. A similar conclusion applies to Bochum 1. On the other hand, New Cluster 1 is among the least massive dynamical survivors of the early phases. However, when only clusters younger than 20 Myr are considered, Bochum 1, and especially New Cluster 1, populate the low-mass tail of the Piskunov et al. (2008) distribution. It is clear that we are dealing with clusters or stellar groups that survived the infanticide phase of embedded clusters (Lada & Lada 2003).

5. Discussion

In this section we compare the properties of the present objects to those of a collection of well-studied OCs analysed by our group following similar methods.

---

[6] Data taken from the VizieR On-line Data Catalog: J/A+A/477/165.

Table 6. Stellar content and mass functions.

		MS					PMS		MS+PMS	
ΔR	Δm_{MS}	N	M	ϕ_0	χ		N	M	N	M
(′)	$(M_\odot)$	(stars)	$(M_\odot)$	(stars $M_\odot^{-1}$)			(stars)	$(M_\odot)$	(stars)	$(M_\odot)$
(1)	(2)	(3)	(4)	(5)	(6)		(7)	(8)	(9)	(10)
				Bochum 1 – Age = 9 ± 3 Myr						
0–3	1.5–8.2	16 ± 2	46 ± 6	17.8 ± 1.5	0.27 ± 0.08		15 ± 8	15 ± 8	31 ± 9	61 ± 10
0–18	1.5–17	128 ± 11	323 ± 29	220 ± 32	0.90 ± 0.12		397 ± 49	397 ± 49	525 ± 55	720 ± 60
				NGC 6823 – Age = 4 ± 2 Myr						
0–1	4.1–27	15 ± 2	158 ± 23	19.5 ± 9.7	0.45 ± 0.26		29 ± 5	29 ± 5	44 ± 6	177 ± 25
0–7	3.5–27	65 ± 4	1046 ± 79	224 ± 49	1.19 ± 0.11		92 ± 20	92 ± 20	157 ± 22	1150 ± 85
				New Cluster 1 – Age = 7 ± 3 Myr						
0–1	1.3–21	10 ± 1	64 ± 11	9.3 ± 3.3	0.25 ± 0.25		10 ± 4	10 ± 4	20 ± 4	74 ± 12

Table notes. Column 1: spatial region where the MF is computed. Column 2: MS mass range. Columns 3–6: stellar content and MF of the MS stars. Columns 7, 8: PMS stellar content. Columns 9, 10: total stellar content.
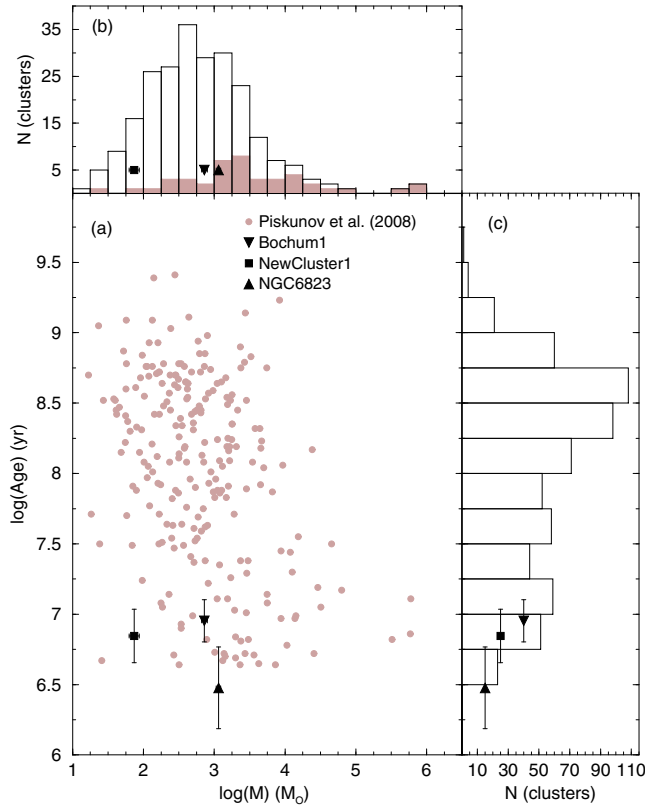
Fig. 11. The age and mass of Bochum 1, New Cluster 1, and NGC 6823 are compared to the set of parameters derived by Piskunov et al. (2008) for a sample of nearby OCs (panel **a)**). Panels **b)** and **c)**: mass and age distributions, respectively. The shaded histogram in **b)** corresponds to clusters younger than 20 Myr.

5.1. Diagnostic diagrams

We further investigate the nature of Bochum 1 (and the other objects in the area) with diagrams that deal with relations among astrophysical parameters of OCs in different environments, which have been introduced by Bonatto & Bica (2005). As reference we use a sample of bright nearby OCs (Bonatto & Bica 2005; Bonatto et al. 2006b), and a group of OCs projected against the central parts of the Galaxy (Bonatto & Bica 2007b).

Also included is the young (∼1.3 Myr) OC NGC 6611 (Bonatto et al. 2006a) for comparison with a gravitationally bound object of similar age. These OCs have ages in the range ∼1.3 Myr to ∼7 Gyr, and Galactocentric distances within $5.8 \lesssim R_{GC}(\text{kpc}) \lesssim 8.1$.

Panels (a) and (b) examine the dependence of cluster (R_{RDP}) and core (R_C) radii on cluster age. While New Cluster 3 and NGC 6823 have R_{RDP} similar to that of NGC 6611 (but apparently smaller than the radii of young OCs), Bochum 1 and New Cluster 1 appear to be abnormally large and small, respectively. A similar relation occurs for the core radii (note that it was not possible to derive R_C for Bochum 1). Most of the small-radii OCs (especially in R_{RDP}) occur at ∼0.5–1 Gyr, the typical time-scale of OC disruption processes near the Solar circle (e.g. Bergond et al. 2001; Lamers et al. 2005).

The core and R_{RDP} of the OCs in the reference sample follow the relation $R_{RDP} = (8.9 \pm 0.3) \times R_C^{(1.0\pm0.1)}$ (panel c). Similar relations between core and RDP radii were also found by Nilakshi et al. (2002), Sharma et al. (2006), and Maciejewski & Niedzielski (2007). Within uncertainties, NGC 6823, New Cluster 3 (and NGC 6611) fit in that relation. The deviant case is again New Cluster 1. The dependence of OC size on Galactocentric distance is suggested by panel (d), as previously discussed by Lyngå (1982) and Tadross et al. (2002). Except for New Cluster 1 and New Cluster 3, the remaining objects follow the trend.

When the mass radial distribution follows a King-like profile (e.g. Bonatto & Bica 2007a; Bonatto & Bica 2008a; Bonatto et al. 2008), the cluster mass inside R_{RDP} can be computed as a function of the core radius (R_C) and the central mass-surface density (σ_{M0}), $M_{clus} = \pi R_C^2 \sigma_{M0} \ln \left[1 + (R_{RDP}/R_C)^2\right]$. With the above relation (panel c) between R_C and R_{RDP}, this equation becomes $M_{clus} \approx 13.8 \sigma_{M0} R_C^2$. The observed relation of core radius and cluster mass is examined in panel (e). The reference OCs, together with NGC 6823, New Cluster 1, and NGC 6611 are contained within King-like mass distributions with central densities within $30 \lesssim \sigma_{M0} (M_\odot \text{ pc}^{-2}) \lesssim 600$. Similarly to the central number-density (Table 5), New Cluster 1 presents one of the lowest central mass densities among the OCs included in Fig. 12.

When the MF slope is considered, Bochum 1 and especially New Cluster 1 appear to have MFs flatter than those of similarly young OCs (panel f). On the other hand, their slopes are equivalent to those derived for some of the old OCs in the reference
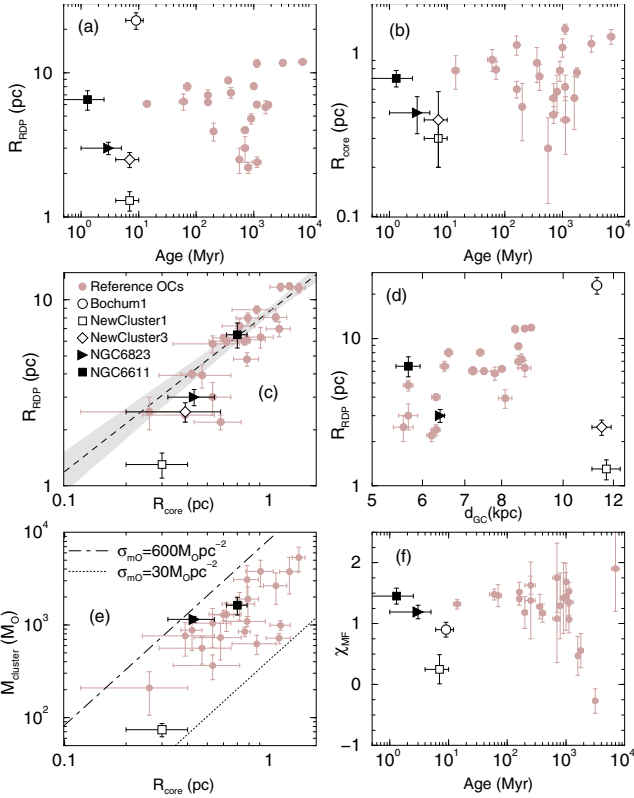
Fig. 12. Relations involving astrophysical parameters of open clusters. Gray-shaded circles: reference OCs. Core radius and cluster (R_{RDP}) size **c)** are related by $R_{RDP} \approx 8.9 R_C$. Core radius and cluster mass **e)** follow the relation $M_{clus} \approx 13.8 \sigma_{M0} R_C^2$.

Fig. 13. Field-decontaminated colour–colour diagrams of the objects. The respective Padova isochrones are shown as a reference for the MS stars.

sample. In most cases, flat MFs reflect advanced dynamical evolution (e.g. Bonatto & Bica 2005).

We conclude that New Cluster 2 is the core of Bochum 1, while New Cluster 1 could be the core of FSR 911, if the latter is confirmed as a stellar system.

5.2. Field-decontaminated colour-colour diagrams

We show in Fig. 13 the $(H - K_s) \times (J - H)$ colour-colour diagrams for the present objects, built with decontaminated photometry to minimise noise. The template NGC 6823 presents well-populated MS and PMS $((J - H) \gtrsim 0.8)$ sequences. Bochum 1 and its neighbours are older than NGC 6823, as denoted by the depletion of PMS stars (Bonatto et al. 2006b). The faint-clump diagram is consistent with being part of the Bochum 1 population surroundings. Since its RDP decays radially, it is an overdensity, which does not exclude the possibility of the clump being a fragment of the Bochum 1 association, or of FSR 911.

Low-mass embedded clusters in general do not harbour any ionising stars (Soares et al. 2005), which appears to be the case of New Cluster 3. They lose important fractions of the primordial mass (Goodwin & Bastian 2006), become gravitationally unstable, and are expected to dissolve on a timescale of a few Myr (Soares et al. 2008; Goodwin & Bastian 2006).

Compact young clusters (CYCs) appear to have survived the gas mass loss during the embedded cluster phase, but they may not live long. Massive ($\gtrsim 25\ M_\odot$) stars formed in massive star clusters will probably end up as low-mass black holes, after the supernova phase. Such massive clusters will probably
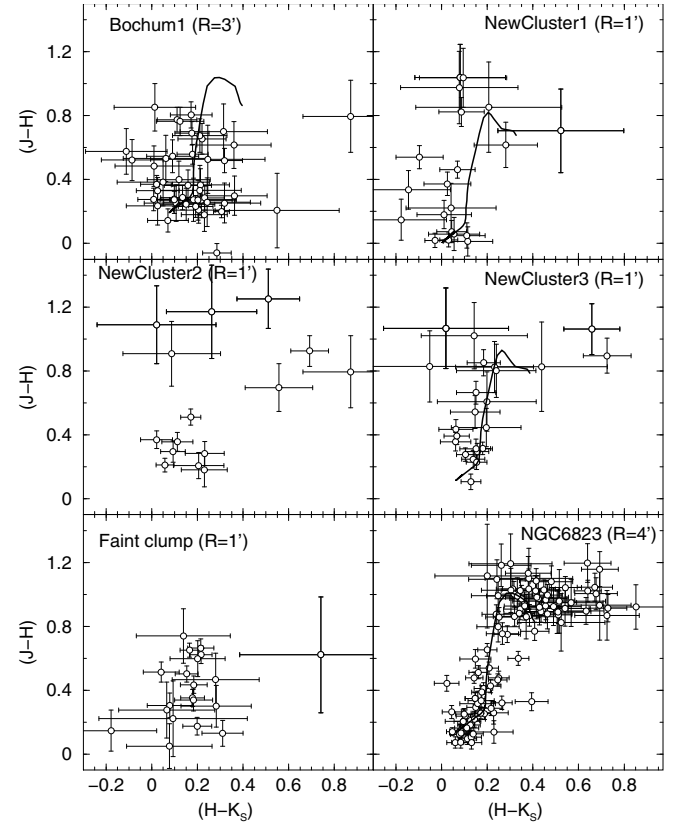
survive dynamically long after the infant-mortality phase (e.g. Goodwin & Bastian 2006). However, CYCs like New Cluster 1 may have a total mass of only $\lesssim 100\ M_\odot$ (Sect. 4). They have late O and B star members (Table 1), with mass in the range 10–25 $M_\odot$. In such cases, supernova explosions will probably produce $\approx 1.4\ M_\odot$ neutron stars as residuals. Two supernovas in such low-mass clusters imply a sudden decrease of the total cluster mass of about 70%, making CYCs instantly unstable. In relative terms, CYCs will undergo more mass loss than massive clusters, leading to a more efficient disruption (e.g. Bonatto & Bica 2007a).

Compact objects such as New Cluster 1 may constitute a new class of star clusters in a young environment, with no evident gas or dust emission. The lack of emission in CYCs is the feature that distinguishes them from the young embedded clusters (e.g. Hodapp 1994).

6. Concluding remarks

Because of its sparse stellar distribution, previous studies have considered Bochum 1 as an OB stellar group, an open cluster, or an association. In the present paper we investigate its nature with field-star decontaminated 2MASS photometry and stellar radial density profiles. With an age of ≈ 3 Myr, the Vul OB1 association, which contains the young OC NGC 6823 and the very compact embedded cluster Cr 404, are used for comparisons with the young stellar content and stellar radial density profiles present in the Bochum 1 area.

As for NGC 6823, conspicuous sequences of MS and PMS stars are present in the decontaminated CMD of Bochum 1,

consistent with the ≈9 Myr of age. However, the RDP of Bochum 1 is irregular and does not follow a King-like profile, which suggests important erosion or dispersion of stars from a possible primordial cluster. The MS and PMS sequences of NGC 6823 produce King-like RDPs, but with a large excess of MS stars near the centre. Unlike Vul Ob1, which includes the H II region Sh2-86, no evident gas emission appears in Bochum 1.

We found two new small compact young clusters in the area of Bochum 1 (one of which may be its remnant core), as well as one embedded cluster. One of the small compact clusters is located ≈8′ to the NW of Bochum 1 (probably the remnant core of a large previous cluster). Together with a clump of faint stars somewhat to the north, both have been taken as the core of an extended cluster (FSR 911). Interestingly, the structure of the two clusters in the Bochum 1 area may have evolved from an interaction, as described by Portegies Zwart & Rusli (2007) for the LMC pair NGC 2136/NGC 2137, and in some SMC cluster pairs (e.g. de Oliveira et al. 2000).

Available evidence shows that structurally, Bochum 1 is not a star cluster. A possible scenario is a fossil remain of a star cluster, as suggested by the core (New Cluster 2) and the radially decaying stellar density profile. In this context, Bochum 1 can be a missing link connecting young star cluster dissolution with the formation of low-mass OB associations. However, the processes that generate large OB associations such as Vul OB1 are yet to be explored in more detail. Probably the difference between objects like Bochum 1, and the star cluster NGC 6823 arises from the mass stored in the objects. On the other hand, the erosion of a primordial cluster is not the only explanation for the irregular radial stellar density profile of Bochum 1. Indeed, star formation may occur along the border of a radially expanding density wave or ionisation front (e.g. Soria et al. 2005; Elmegreen & Lada 1977). In some cases, the neutral interstellar medium can be compressed by the expanding bubble above the stability criterion against gravitational collapse, which could trigger localised star formation, giving rise to a clumpy radial density profile.

The two compact New Clusters 1 and 2, and the embedded New Cluster 3, are new findings in the area of Bochum 1 and FSR 911. We show that Bochum 1 and FSR 911 are different objects. The optically identified small object New Cluster 1 and the large infrared overdensity (Fig. 1 and Table 1) may be the same object. However, probably because of the lack of decontamination, Froebrich et al. (2007) overestimated the dimensions of FSR 911. The whole ensemble may turn out to be a Rosetta Stone to decode early-dynamical evolution processes involving embedded clusters, young compact clusters, open clusters and associations. Theoretical evidence in favour of clusters as cores of expanding associations has been presented by Kroupa et al. (2001) and Kroupa (2005). However, to unravel all evolutionary connections we probably must wait for Gaia's[7] deep proper motions.

---

[7] http://www.rssd.esa.int/index.php?project=Gaia

References

Albacete Colombo, J. F., Flaccomio, E., Micela, G., Sciortino, S., & Damiani, F. 2007, A&A, 464, 211

Barkhatova, K. A. 1957, SvA, 1, 822

van den Bergh, S., Morbey, C., & Pazder, J. 1991, ApJ, 375, 594

Bergond, G., Leon, S., & Guilbert, J. 2001, A&A, 377, 462

Bica, E., Bonatto, C., Barbuy, B., & Ortolani, S. 2006, A&A, 450, 105

Bica, E., Bonatto, C., & Camargo, D. 2008, MNRAS, 385, 349

Blaauw, A. 1964, ARA&A, 2 , 213

Bonatto, C., & Bica, E. 2005, A&A, 437, 483

Bonatto, C., & Bica, E. 2006, A&A, 460, 83

Bonatto, C., & Bica, E. 2007a, A&A, 473, 445

Bonatto, C., & Bica, E. 2007b, MNRAS, 377, 1301

Bonatto, C., & Bica, E. 2008a, A&A, 477, 829

Bonatto, C., & Bica, E. 2008b, A&A, 485, 81

Bonatto, C., Bica, E., & Girardi, L. 2004, A&A, 415, 571

Bonatto, C., Santos Jr., J. F. C., & Bica, E. 2006a, A&A, 445, 567

Bonatto, C., Bica, E., Ortolani, S., & Barbuy, B. 2006b, A&A, 453, 121

Bonatto, C., Bica, E., & Santos Jr., J. F. C. 2008, MNRAS, 386, 324

Brand, J., & Blitz, L. 1993, A&A, 275, 67

Cardelli, J. A., Clayton, G. C., & Mathis, J. S. 1989, ApJ, 345, 245

Carraro, G., Janes, K. A., Costa, E., & Méndez, R. A. 2006, MNRAS, 368, 1078

Collinder, P. 1931, AnLun, 2, 1

Dias, W. S., Alessi, B. S., Moitinho, A., & Lépine, J. R. D. 2002, A&A, 389, 871

Dutra, C. M., Santiago, B. X., & Bica, E. 2002, A&A, 383, 219

Efremov, Y. N., & Elmegreen, B. G. 1998, MNRAS, 299, 588

Elmegreen, B. G., & Lada, C. J. 1977, ApJ, 214, 725

Froebrich, D., Scholz, A., & Raftery, C. L. 2007, MNRAS, 374, 399

de la Fuente Marcos, R., & de la Fuente Marcos, C. 2008, ApJ, 672, 342

Girardi, L., Bertelli, G., Bressan, A., et al. 2002, A&A, 391, 195

Goodwin, S. P., & Bastian, N. 2006, MNRAS, 373, 752

Hodapp, K.-W. 1994, ApJS, 94, 615

Kharchenko, N. V., Piskunov, A. E., Röser, S., Schilbach, E., & Scholz, R.-D. 2005, A&A, 438, 1163

King, I. 1962, AJ, 67, 471

Knödlseder, J. 2000, A&A, 360, 539

Kroupa, P., Aarseth, S., & Hurley, J. 2001, MNRAS, 321, 699

Kroupa, P. 2005, in The Three-Dimensional Universe with Gaia, Observatoire de Paris-Meudon, 4–7 October 2004, ed. C. Turon, K. S. O'Flaherty, & M. A. C. Perryman, 629

Lada, C. J., & Lada, E. A. 2003, ARA&A, 41, 57

Lamers, H. J. G. L. M., Gieles, M., Bastian, N., et al. 2005, A&A, 441, 117

Lyngå, G. 1982, A&A, 109, 213

Maciejewski, G., & Niedzielski, A. 2007, A&A, 467, 1065

Maíz-Apellániz, J. 2001, ApJ, 560, L83

Massey, P., Johnson, K. E., & De Gioia-Eastwood, K. 1995, ApJ, 454, 151

Mercer, E. P., Clemens, D. P., Meade, M. R., et al. 2005, ApJ, 6335, 560

Mermilliod, J. C., & Paunzen, E. 2003, A&A, 410, 511

Moffat, A. F. J., & Vogt, N. 1975, A&AS, 20, 85

Nilakshi, S. R., Pandey, A. K., & Mohan, V. 2002, A&A, 383, 153

de Oliveira, M. R., Bica, E., & Dottori, H. 2000, MNRAS, 311, 589

Pigulski, A., Kolaczkowski, Z., & Kopacki, G. 2000, AcA, 50, 113

Piskunov, A. E., Kharchenko, N. V., Röser, S., Schilbach, E., & Scholz, R.-D. 2006, A&A, 445, 545

Piskunov, A. E., Schilbach, E., Kharchenko, N. V., Röser, S., & Scholz, R.-D. 2008, A&A, 477, 165

Portegies Zwart, S. F., & Rusli, S. P. 2007, MNRAS, 374, 931

Salpeter, E. E. 1955, ApJ, 121, 161

Sharma, S., Pandey, A. K., Ogura, K., et al. 2006, AJ, 132, 1669

Sharpless, S. 1959, ApJS, 4, 257

Siess, L., Dufour, E., & Forestini, M. 2000, A&A, 358, 593

Soares, J. B., Bica, E., Ahumada, A. V., & Clariá, J. J. 2005, A&A, 430, 987

Soares, J. B., Bica, E., Ahumada, A. V., & Clariá, J. J. 2008, A&A, 478, 419

Soria, R., Cropper, M., Pakull, M., Mushotzky, R., & Wu, K. 2005, MNRAS, 356, 12

Stephenson, C. B., & Sanduleak, N. 1971, Publ. Warner & Swasey Obs., 1, 1

Tadross, A. L., Werner, P., Osman, A., & Marie, M. 2002, NewAst, 7, 553

Torres, C. A. O., da Silva, L., Quast, G. R., de la Reza, R., & Jilinski, E. 2000, AJ, 120, 1410

Trager, S. C., King, I. R., & Djorgovski, S. 1995, AJ, 109, 218

Yadav, R. K. S., & Sagar, R. 2003, BASI, 31, 87

Yonekura, Y., Asayama, S., Kimura, K., et al. 2005, ApJ, 634, 476